Available online at www.sciencedirect.com
SCIENCE DIRECT®
ELSEVIER
Journal of Magnetism and Magnetic Materials 293 (2005) 872–879
Journal of magnetism and magnetic materials
www.elsevier.com/locate/jmmm

Effect of Ni doping in rare-earth manganite $La_{0.7}Pb_{0.3}Mn_{1-x}Ni_xO_3$ ($x = 0.0-0.5$)

Sudipta Pal[a,*], Esa Bose[a], B.K. Chaudhuri[a], H.D. Yang[b], S. Neeleshwar[c], Y.Y. Chen[c]

[a]*Department of Solid State Physics, Indian Association for The Cultivation of Science, Kolkata 700032, India*
[b]*Department of Physics, National Sun Yat Sen University, Kaohsiung 804, Taiwan, ROC*
[c]*Institute of Physics, Academia Sinica, Taipei, Taiwan, ROC*

Received 26 September 2004; received in revised form 2 November 2004
Available online 24 December 2004

Abstract

With Ni doping, $La_{0.7}Pb_{0.3}Mn_{1-x}Ni_xO_3$ ($x = 0-0.5$) system exhibits decrease of conductivity and increase of metal–insulator transition temperature. This is considered to occur because of the decrease of effective double exchange (DE) interaction due to Ni doping. The presence of majority of Ni^{2+} states as indicated by the XPS study, govern the transport and magnetic properties of this system. The spin-wave stiffness constant D, characterising the magnon in the low-temperature ($T < T_p$) ferromagnetic phase, estimated from the magnetisation (M) data, decreases with increasing Ni content. Unlike spin-glass-like pure insulating state below the Curie Temperature (T_C), observed in other similar transition metal ion-doped systems, magnetisation (both zero field cooled (ZFC) and field cooled (FC) measured down to 10 K) and resistivity data of the samples indicate the existence of ferromagnetic cluster-like-state, which becomes more vivid with increasing Ni doping. Like many other colossal magnetoresistive (CMR) systems, small polaron hopping conduction is observed in the high-temperature ($T > T_p$) semiconducting phase showing increase of activation energy as conductivity decreases.

PACS: 75.47.Gk; 72.10.Di; 75.30.Ds

Keywords: Ni doping; Ferromagnetic-cluster; Colossal magnetoresistance; Spin-wave stiffness constant; Electron-magnon scattering

1. Introduction

Doping of transition metal ions (viz. Fe, Cr, Ni, etc.) at the Mn site [1–6] of colossal magnetoresistive (CMR) manganites is an interesting topic of study. Small change in the Mn^{3+}–O–Mn^{4+}

*Corresponding author. Tel.: +91 33 247 34971; fax: +91 33 247 32805.
E-mail address: sudipta.pal@rediffmail.com (S. Pal).

0304-8853/$ - see front matter © 2004 Elsevier B.V. All rights reserved.
doi:10.1016/j.jmmm.2004.12.005

network caused by transition metal ion substitution results in large changes in the magnetic and transport properties of such systems. Among the transition metal ion family, Nickel is one of the most fascinating members [7–9]. It has been observed that Ni doping at Mn site weakens ferromagnetism in the manganite system [10,11]. Substitution of Mn by Ni destroys the long-range ferromagnetic order and induces a spin-glass-like pure insulating state in the La–Sr–Mn–O system [12]. In case of Mn substitution by Ni, the combination of Ni^{2+} and Mn^{4+} has been observed to be favourable [13–15]. In the present investigation, Mn has been substituted by Ni in $La_{0.7}Pb_{0.3}MnO_3$ to study the change in the low-temperature ferromagnetic behaviour. The XPS study has been used to determine the ionic state of Ni in these compounds.

Earlier investigation of the La–Pb–Mn–O system by neutron scattering measurement shows the presence of well-defined spin waves or magnon throughout the Brillouin zone [16] at low temperature. Calculation of spin-wave stiffness constant (D) from the temperature-dependent magnetisation data also gives important information regarding the strength of microscopic magnetic coupling of the spins associated with the ferromagnetic clusters in the low-temperature [17] region. It is well known that below the Curie temperature T_C, $La_{0.7}Pb_{0.3}MnO_3$ behaves like a double-exchange (DE)-type ferromagnet. So a detailed analysis of low-temperature magnetisation data would help to throw more light on the behaviour of magnetic coupling of the spins and the importance of magnons in these DE-type ferromagnets. The Ni-doped manganite system is of particular interest for investigating the change in the spin-wave stiffness constant (D) due to weakening behaviour of the effective ferromagnetic DE interaction [11,12].

In the present work, the Ni-doped $La_{0.7}Pb_{0.3}Mn_{1-x}Ni_xO_3$-type CMR system has been carefully prepared and well characterised by structural and XPS studies. Low-temperature magnetisation and transport properties (viz. TEP and resistivity) have been measured showing the importance of electron-magnon scattering and the presence of ferromagnetic cluster-like state in the low-temperature metallic phase. High-temperature ($T > T_p$) resistivity data have been analysed to illustrate the nature of conduction mechanism in this Ni-doped system.

2. Experimental

For the preparation of bulk $La_{0.7}Pb_{0.3}Mn_{1-x}Ni_xO_3$ ($0.0 < x < 0.5$), the standard solid state reaction technique similar to our earlier work [6] has been followed. Stoichiometric amounts of La_2O_3, PbO, $Mn(C_2H_3O_2)_2$ and $Ni(NO_3)_2 \cdot 6H_2O$ (each of purity 99.99%) were taken as the starting materials. The mixtures of these raw materials were preheated in air at 773 K for 5 h. After grinding they were sintered at 1173 K for 40 h with intermediate grinding (four times). The powders of different samples thus obtained were well ground again and then pelletised and finally annealed at 1173 K for 24 h. Finally, the samples were furnace cooled to room temperature. All the samples were characterised by X-ray diffraction (XRD) with CuK_α (wavelength $\lambda = 1.541$ Å) radiation. Rietveld analysis of the diffraction data was performed using the DBWS program. Magnetisation was measured using a SQUID magnetometer down to 4 K in different magnetic fields both in field cooled (FC) and zero field cooled (ZFC) conditions. Temperature-dependent resistivity measurements (ρ) and thermoelectric power measurement were carried out using standard techniques [6] in the range of 80–425 K in 0 and 1.5 T magnetic field. All the experimental data were collected in the heating direction. Room temperature XPS (AXIS-His, KRATOS ANALYTICAL Ltd. UK) spectra were studied to confirm the ionic state of Ni.

3. Results and discussion

Room temperature XRD data of the $La_{0.7}Pb_{0.3}Mn_{1-x}Ni_xO_3$ ($x = 0.0-0.5$) system indicate rhombohedral space group ($R\bar{3}c$) with hexagonal setting ($Z = 6$). The substitution of Mn by Ni ion produces only a minor distortion in the MnO_6 octahedra. The changes in the Mn–O–Mn angles are also small (164–166° for $x = 0.0-0.5$).

Moreover, the tolerance factor (t) of the perovskite structure [$t = (d_{La-O}/\sqrt{2}(d_{Mn-O})$, where d_{La-O} and d_{Mn-O} are the La–O and Mn–O bond distances] remains almost unchanged (~0.99) for the samples with different concentrations of Ni. The Mn/Ni–O bond distance as well as the unit-cell volume, however, decreases slightly (from 1.969 to 1.953 Å for $x = 0.0$ to $x = 0.5$), which might be due to a smaller ionic radii of Ni^{2+} compared to Mn^{3+}. This observation of structural behaviour agrees well with the earlier reports of Ni-doped systems [18]. The peak in the XPS spectra (Fig. 1) shows Ni $2p_{3/2}$ edges of a typical sample $La_{0.7}Pb_{0.3}Mn_{0.6}Ni_{0.4}O_3$. Considering similar spectra observed earlier [19,20], it can be inferred that the ionic state of Ni in the present compounds is mainly Ni^{2+}. It is worth mentioning here that earlier the presence of Ni^{3+} was assumed in the Ni-doped La–Sr–Mn–O system, but was not confirmed by XPS or other studies [12].

The results of magnetisation measurement of the samples in different fields (1000, 100 Oe) both in FC and ZFC processes have been shown in Figs. 2 and 3, respectively. The FC magnetisation curve (Fig. 2) indicates that all the Ni-doped samples undergo a paramagnetic to ferromagnetic transition with lowering of temperature. As Ni concentration increases, both Curie temperature T_C and magnetisation M decrease simultaneously. It is very difficult to get a clear idea about the charge distribution and exchange interactions in the Ni-doped compounds. However, it can be assumed that some of the Ni^{2+} ions are surrounded by Ni^{2+} ions; similarly, some of the Mn^{4+} ions are surrounded by Mn^{4+} ions which are coupled antiferromagnetically with the nearest neighbours. The increasing number of Ni^{2+}–O–Ni^{2+} and Mn^{4+}–O–Mn^{4+} interactions also contribute in decreasing Curie temperature and spontaneous magnetisation. The contribution of the Ni^{2+}–O–Mn^{4+} ferromagnetic superexchange interaction in the net magnetisation should also be taken into account. However, it has been observed that both Curie temperature T_C and magnetisation M decrease simultaneously with Ni doping. Fig. 3a shows that the FC and ZFC data do not coincide just below T_C, indicating the presence of some randomly frozen-in magnetic clusters. The bifurcation between ZFC and FC data (Fig. 3a) disappears when higher magnetic field is applied (Fig. 2), showing the existence of field-induced ferromagnetic order in the magnetic domains. Interestingly, unlike the Ni-doped La–Sr–Mn–O system [12] or Cr-doped La–Pb–Mn–O system [6], the spin-glass-like pure insulating state has not been observed in the Ni-doped $La_{0.7}Pb_{0.3}MnO_3$

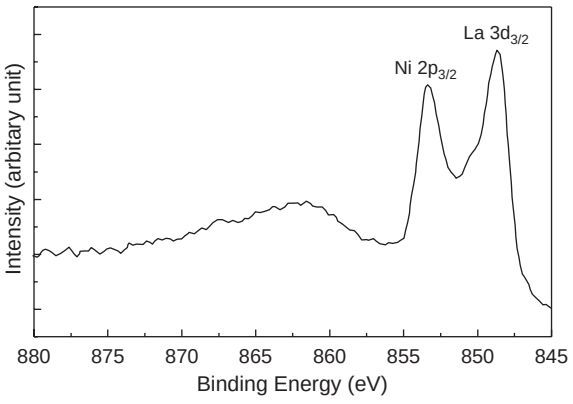

Fig. 1. Room temperature XPS spectra showing Ni $2p_{3/2}$ and La $3d_{3/2}$ edges of $La_{0.7}Pb_{0.3}Mn_{0.6}Ni_{0.4}O_3$, peak position indicating the presence of majority Ni^{2+} states.

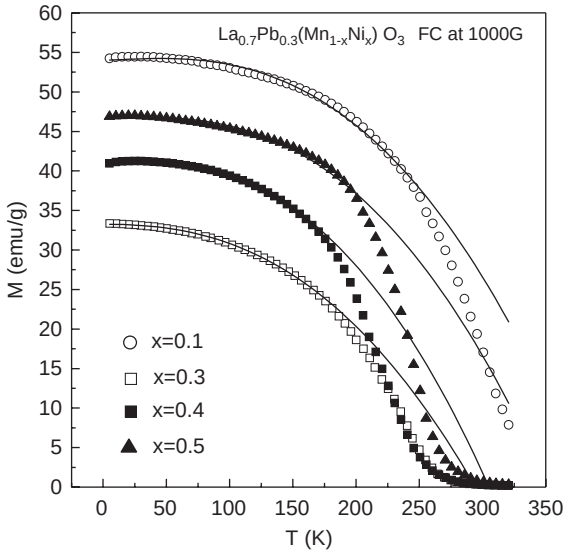

Fig. 2. Temperature dependence of magnetisation in FC process with applied field 1000 Oe for the samples $La_{0.7}Pb_{0.3}Mn_{1-x}Ni_xO_3$ ($x = 0.1,0.3,0.4,0.5$). Solid lines are best-fitted curves using Eq. (1).

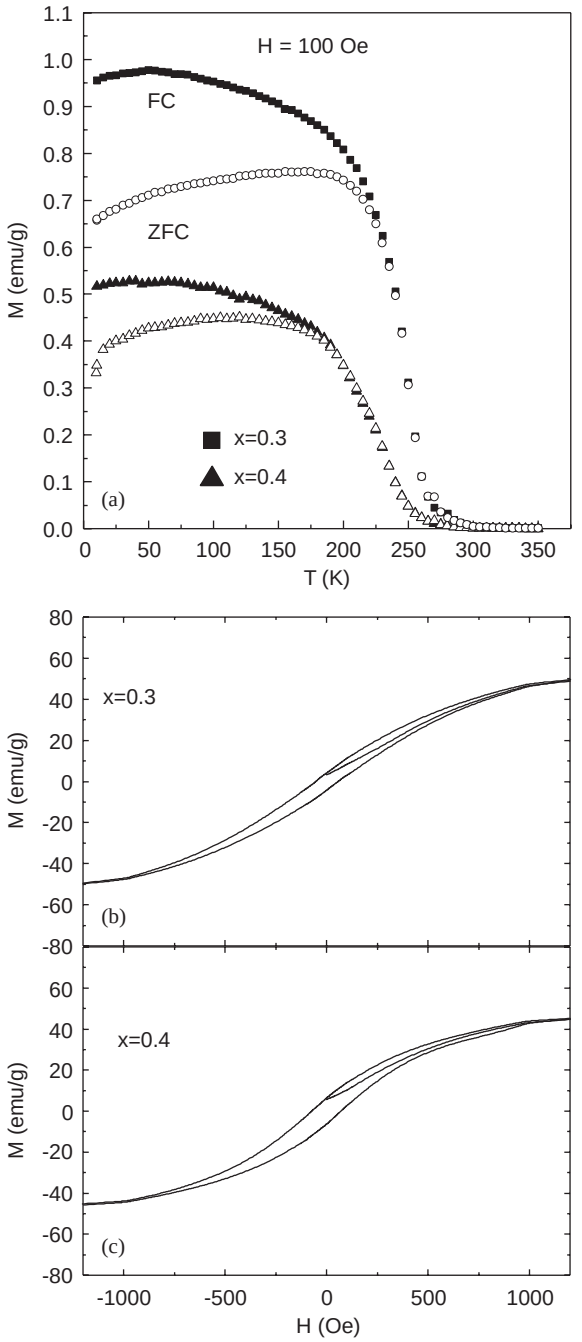

Fig. 3. (a) Temperature dependence of magnetisation in ZFC and FC processes with applied fields 100 Oe for the samples $La_{0.7}Pb_{0.3}Mn_{1-x}Ni_xO_3$ ($x = 0.3,0.4$). The noncoincident FC and ZFC data below T_C indicate the presence of some randomly frozen-in magnetic clusters (b) and (c). The field dependence (up to 6 T) of magnetisation measured at 5 K of the same samples showing small hysteresis at low field (below 1000 Oe).

system of our present investigation. The field dependence (up to 6 T) of magnetisation measured at 5 K shows small hysteresis (Fig. 3b,c) at sufficiently low field (below 1000 Oe). The hysteresis in this material is considered to be due to some anisotropy energy of the clusters/domains. The small increase in coercive field (–60 Oe for $x = 0.3$ and -80 Oe for $x = 0.4$) with Ni doping appears to be associated with the increase of anisotropic nature of the magnetic domain.

The strength of the microscopic magnetic coupling of the spins associated with the ferromagnetic clusters can be estimated from the measurement of ferromagnetic spin-wave stiffness constant (D) [17,23]. Within the spin-wave approximation, the low-temperature magnetisation is given by the relation

$$M(T) = M(0) - BT^{3/2} - CT^{5/2}, \quad (1)$$

where $B = 0.0587\, g\mu_B(k_B/D)$ and C is a constant. At a temperature one order of magnitude lower than the Curie temperature, the second term dominates. But at $T_C/2$, higher power terms take over and magnetisation vanishes abruptly at T_C, deviating from the Heisenberg-like behaviour. Solid lines in Fig. 2 show best-fitted curves following Eq. (1). The stiffness constant D of the sample has been determined from the fitting of magnetisation data with Eq. (1) in a field of 1000 Oe. The estimated D value ($= 160.18$ meV Å^2) is in good agreement with the previously reported result [21]. With the increase of Ni doping, D values decrease ($D = 151.52$, 134.67 and 99.94 meV Å^2, for $x = 0.3$, 0.4 and 0.5, respectively) which indicates the decrease of the strength of magnetic coupling in the ferromagnetic clusters with Ni doping. Theoretical calculation, taking into account superexchange and DE present in the system however, would give closer value to the experimental data.

Fig. 4 shows the thermal variation of resistivity (ρ) of $La_{0.7}Pb_{0.3}Mn_{1-x}Ni_xO_3$ ($x = 0.0-0.5$). The zero-field resistivity increases with the increase of Ni concentration. The metal–insulator transition temperature T_p shifts towards lower temperature with the increase of resistivity and Ni concentration. For the samples with $x > 0.3$, the low-temperature insulating-like phase seems to exhibit

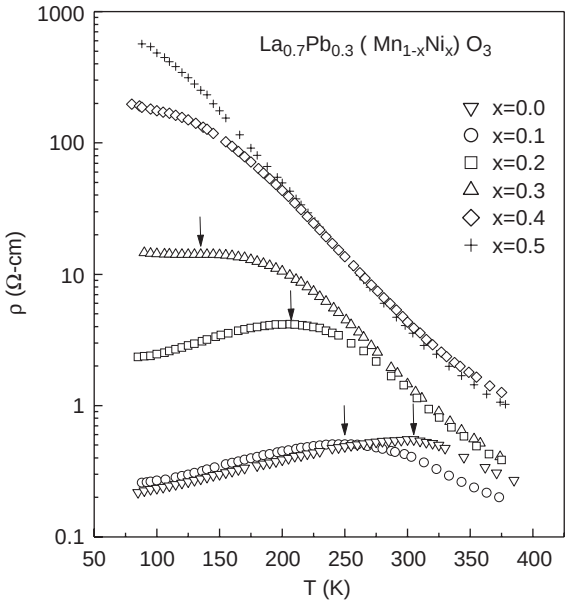

Fig. 4. Thermal variation of zero field resistivity (ρ) of $La_{0.7}Pb_{0.3}Mn_{1-x}Ni_xO_3$ with $x = 0.0-0.5$. No pure insulating state has been observed even up to an Ni concentration $x = 0.5$. Corresponding T_p is marked with arrows.

the magnetic cluster-like behaviour [12] as observed from the magnetisation measurement. It is well known that the ferromagnetism and metallic conductance are the result of DE interaction between Mn^{3+} and Mn^{4+} ions in the divalent-doped rare-earth manganite [22]. When Ni ion occupies the Mn ion site in the lattice, there is no DE interaction between neighbouring Ni ions and hence ferromagnetism decreases. The resultant exchange interaction (discussed in earlier section) also favours the decrease in ferromagnetism in the system. So, with the increase of Ni content in the sample, the number of ferromagnetic clusters increases and ferromagnetic metallic continuum region decreases. Only some isolated ferromagnetic clusters can form in the magnetically disordered region. In this case, the conductance is controlled by the electron transport across the insulating regime and the conductivity decreases. For our present system, it is worthwhile to mention that a pure spin-glass-like insulating behaviour has not been observed from the resistivity data even for the sample with maximum Ni doping ($x = 0.5$), whereas it has been observed in the Cr-doped $La_{0.5}Pb_{0.5}MnO_3$ system [6]. We consider strong ferromagnetic ordering in the $La_{0.7}Pb_{0.3}MnO_3$ system responsible for the disappearance of spin-glass-like insulating state even for the sample with highest Ni doping ($x = 0.5$) in the present system of our investigation.

To find the conduction mechanism, conductivity data (Fig. 5) above and below T_p have been analysed considering different interaction mechanisms. Resistivity data of the samples with $x < 0.3$ show metallic behaviour below T_p. In the metallic phase ($T < T_p$), resistivity data of the present samples follow the relation

$$\rho = \rho_\alpha + \rho_{2.5}T^{2.5}, \tag{2}$$

where the first term ρ_α corresponds to resistivity arising due to domain, grain boundary and other temperature-independent scattering mechanisms [24–27]. The $\rho_{2.5}T^{2.5}$ term appears due to electron-magnon scattering [18], which is important in the low-temperature region (below T_p). The low-temperature $\rho - T^{2.5}$ curve shown in Fig. 5 is almost linear suggesting that in the metallic regime transport mechanism can be attributed to the electron-magnon scattering process, which further demonstrates [24] that this region corresponds to ferromagnetic phase. It is interesting to note that the resistivity ($\rho - T$) curves of the samples with lower Ni concentration ($x = 0.1$ and 0.2) are better fitted with Eq. (1) than that of the undoped ($x = 0.0$) sample. This indicates that with increasing Ni concentration and hence with the increase of resistivity, electron-magnon scattering contribution to the resistivity data becomes predominant. The parameters, obtained from best fitting of the low-temperature metallic part of the resistivity data with Eq. (2), are shown in Table 1 (both in 0 and 1.5 T magnetic field). It is found from this table that ρ_α (temperature-independent term) decreases significantly with magnetic field, but the influence of the magnetic field on the $\rho_{2.5}$ term is very small. The decrease of ρ_α in magnetic field appears to be related to the magnetoresistive behaviour of the samples arising due to the alignment of spins in the magnetic domains. As the magnetic field increases, the size of the ferromagnetic domain increases and ρ_α becomes smaller [26]. High-temperature ($T > T_p$) resistivity

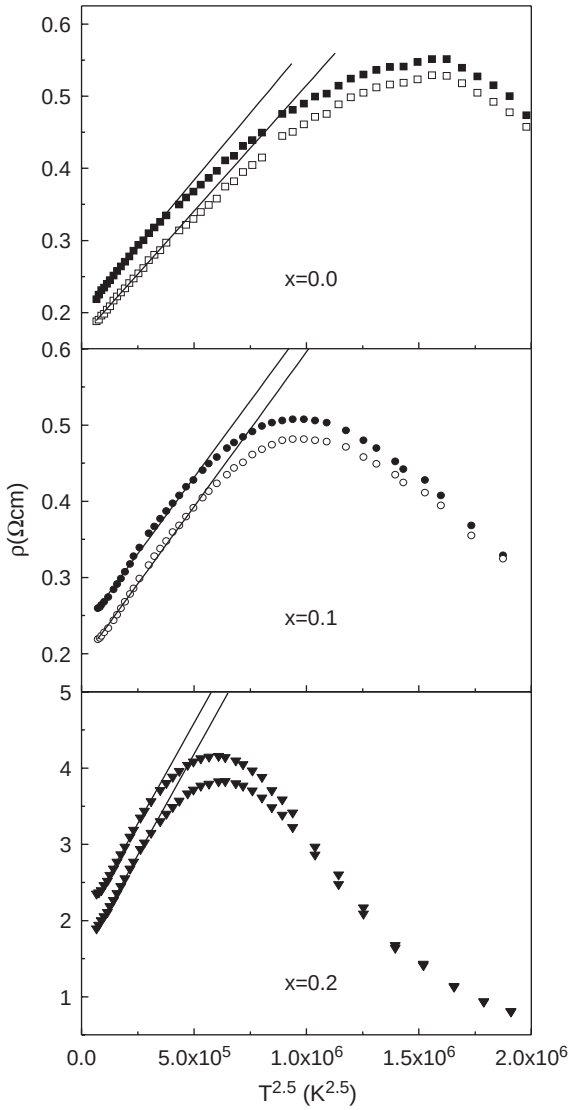

Fig. 5. Resistivity (ρ) vs. $T^{2.5}$ curve for $La_{0.7}Pb_{0.3}Mn_{1-x}Ni_xO_3$ with $x = 0.0,0.1,0.2$ (showing distinct metallic behaviour below T_p) in magnetic field $B = 0.0$ T (solid symbol) and 1.5 T (open symbol). The solid lines give the best-fit curves using Eq. (2) at lower temperatures ($T < T_p$).

data of the semiconducting phase are well fitted with the small-polaron-hopping model (SPH). The expression for conductivity derived from this model can be written [28] as

$$\sigma(T) = \frac{\sigma_0}{T}\exp\left(-\frac{E_p}{k_B T}\right), \quad (3)$$

Table 1
The values of the parameters ρ_0 and $\rho_{2.5}$ obtained from fitting the low-temperature ($T < T_p$) resistivity data using Eq. (2) both in the presence and absence of magnetic field for the samples $La_{0.7}Pb_{0.3}Mn_{1-x}Ni_xO_3$ ($x = 0.0 - 0.2$)

x	ρ_α (Ω cm)		$\rho_{2.5}$ (Ω cm K$^{-2.5}$)	
	0 T	1.5 T	0 T	1.5 T
0.0	0.1977	0.1662	3.71e−7	3.48e−7
0.1	0.2304	0.1900	4.03e−7	4.04e−7
0.2	1.9433	1.5247	6.15e−6	6.27e−6

where σ_0 is a constant, E_p is the total activation energy of a polaron. The activation energy of the sample (Table 2) estimated from the slope of the $\ln \sigma T - (1000/T)$ curve (Fig. 6) increases gradually with increasing Ni content which is due to the increased localisation of the e_g^1 electron of Mn^{3+}.

Fig. 7 shows the thermal variation of Seebeck coefficient (S) for the samples with different concentrations of Ni. The small changes in the electronic structure due to the presence of Ni affect the thermoelectric power. Interestingly, the value of S is negative for all the samples in the entire temperature range of our measurement (80–320 K) which might be due to n-type charge carriers present in the Ni-doped samples similar to that of the undoped ($x = 0$) sample. However, Hall effect study would give more accurate conclusion. The magnitude of S also increases with the increase of Ni doping similar to the corresponding increase of resistivity (Fig. 5) predicting the importance of impurity scattering with increasing Ni ions. Moreover, with the increase of Ni^{2+} and Mn^{4+} ions, the effective DE interaction becomes weaker, resulting in the decrease of the only electronically active e_g^1 electron of Mn^{3+}, which causes the gradual shift of S towards the higher negative value.

The thermoelectric power data in the FM phase both in presence and in absence of magnetic field cannot be fitted well with two-band model [29]. The TEP data can, however, be well analysed with an expression [18] of the form

$$S = S_0 + S_{3/2}T^{3/2} + S_4 T^4, \quad (4)$$

Table 2
Different parameters (E_p from Eq. (3) and S_0, $S_{3/2}$,S_4 from Eq. (4)) regarding transport properties estimated from conductivity and thermoelectric power of $La_{0.7}Pb_{0.3}Mn_{1-x}Ni_xO_3$ ($x = 0.0-0.5$)

x	T_P	E_p (meV)	S_0	$S_{3/2}$	S_4
0.0	310	122.60	0.43	5.6×10^{-4}	-9.37×10^{-10}
0.1	250	127.16	−1.38	15.0×10^{-4}	-1.72×10^{-9}
0.2	206	173.93	−3.69	27.9×10^{-4}	-3.07×10^{-10}
0.3	135	181.38	−5.18	32.7×10^{-4}	-3.58×10^{-10}
0.4	—	188.05	—	—	—
0.5	—	190.61	—	—	—

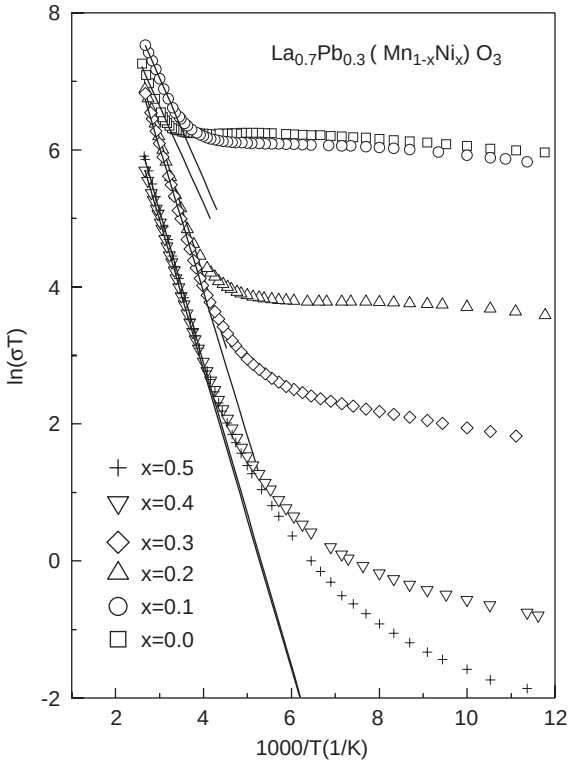

Fig. 6. Variation of $\ln \sigma T$ as a function of $1000/T$ for $La_{0.7}Pb_{0.3}Mn_{1-x}Ni_xO_3$ with $x = 0.0-0.5$, above the metal–insulator transition temperature. Solid lines are the best-fit curves corresponding to the Mott's SPH model (Eq. (3)).

where S_0 term (S at $T = 0\,K$) has no physical origin. The $T^{3/2}$ behaviour suggests that electron-magnon scattering strongly affects the low-temperature (FM phase) TEP data of this type of manganites as also observed in the case of

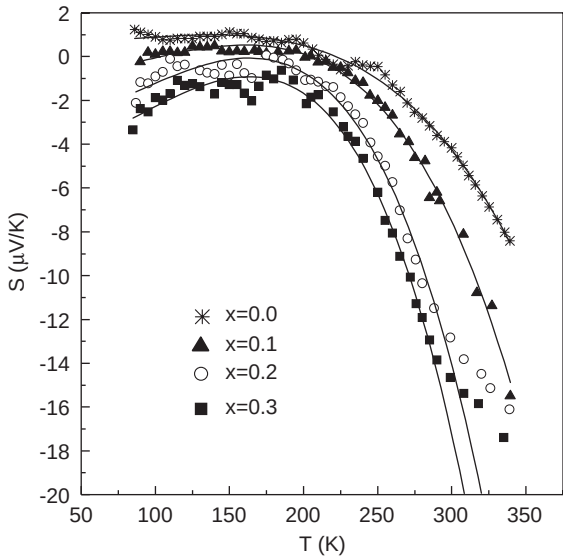

Fig. 7. Thermal variation of Seebeck coeffecient (S) of $La_{0.7}Pb_{0.3}Mn_{1-x}Ni_xO_3$ with $x = 0.0-0.3$. The samples with $x > 0.3$ could not be measured throughout the temperature range due to the fluctuation of the thermo-emf. Solid lines are best-fitted curves using Eq. (4).

temperature-dependent resistivity behaviour. The solid lines in Fig. 7 show the best-fitted curves using Eq. (4). Increase of Ni concentration increases the value of $S_{3/2}$ consistently (Table 2), indicating the increase of electron-magnon scattering, as the spin-wave coupling strength decreases. The origin of the S_4T^4 term is still not clear. It may be due to spin-wave fluctuation in the FM phase, as discussed by Urushibara et al. [30] to explain their low-temperature conductivity data. At higher temperature this term cannot be neglected. Though several authors [27,30] obtain an additional $T^{4.5}$ (spin-wave scattering) contribution to explain conductivity data [6], no such additional temperature dependence has been mentioned by us while explaining the corresponding low-temperature data in the FM phase of all the La–Pb–MnO samples.

4. Conclusion

In summary, effects of Ni doping on magnetisation and magnetotransport properties of the

$La_{0.7}Pb_{0.3}Mn_{1-x}Ni_xO_3$ ($x = 0.0-0.5$) system have been investigated in detail. Little change of lattice parameters and presence of Ni^{2+} state are concluded, respectively, from the XRD and XPS studies. The magnetisation data reveal the existence of spin waves or magnon excitation. Temperature-dependent resistivity and thermoelectric power data also support the existence of the electron-magnon scattering in this system. Ni doping at the Mn site causes the modification of Mn–O–Mn network, which weakens ferromagnetism and resistivity increases. Low-temperature (below T_C) magnetisation (both in ZFC and FC) and resistivity data show a ferromagnetic-cluster-like behaviour in the samples. The system does not show spin-glass-like insulating behaviour even for highest Ni concentration ($x = 0.5$) of our present investigation. The decreasing value of spin-wave stiffness constant (D) supports the decrease of the strength of the microscopic magnetic coupling of the spins associated with the ferromagnetic clusters with increase of Ni concentration in this system.

References

[1] M. Jaime, M.B. Salamon, M. Rubienstein, R.E. Treece, J.S. Horwitz, D.B. Chrisey, Phys. Rev. B 54 (1996) 11914.
[2] P.V. Vanitha, R.S. Singh, S. Natarajan, C.N.R. Rao, Solid State Commun. 109 (1999) 135.
[3] A. Maignan, C. Martin, F. Damay, M. Hervieu, B. Raveau, J. Magn. Magn. Mater. 188 (1998) 185.
[4] L. Pi, L. Zhang, Y. Zhang, Phys. Rev. B 61 (2000) 8917.
[5] X.W. Cao, J. Fang, K.B. Li, Solid State Commun. 115 (2000) 201.
[6] A. Banerjee, S. Pal, B.K. Chaudhuri, J. Chem. Phys. 115 (2001) 1550.
[7] E. Banks, N. Tashima, J. Appl. Phys. 41 (1970) 1186.
[8] J. Blasco, J. García, J.M. de Teresa, M.R. Ibarra, J. Perez, P.A. Algarabel, C. Marquina, C. Ritter, Phys. Rev. B 55 (1997) 8905.
[9] L. Righi, P. Gorria, M. Insausti, J. Gutiérrez, J.M. Barandiarán, J. Appl. Phys. 81 (1997) 5767.
[10] J.B. Goodenough, A. Wold, R.J. Arnott, N. Menyuk, Phys. Rev. 124 (1961) 373.
[11] J. Gutierrez, A. Pena, J.M. Barandiaran, J.L. Pizarro, L. Lezama, M. Insausti, T. Rojo, J. Phys.: Condens. Matter 12 (2000) 10523.
[12] Ji-Wen Feng, C. Ye, L.-P. Hwang, Phys. Rev. B 61 (2000) 12271.
[13] J. Blasco, M.C. Sánchez, J. Pérez-Cacho, J. García, G. Subías, J. Campo, J. Phys. Chem. Solids 63 (2002) 781.
[14] O. Toulemonde, F. Studer, B. Raveau, Solid State Commun. 63 (2002) 781.
[15] M.C. Sánchez, J. García, J. Blasco, G. Subías, J. Perez-Cacho, Phys. Rev. B 65 (2002) 144409.
[16] T.G. Rerring, G. Aeppli, S.M. Hayden, S.A. Carter, J.P. Remeika, S.W. Cheong, Phys. Rev. Lett. 77 (1996) 711.
[17] M. Jaime, P. Lin, M.B. Salamon, P.D. Han, Phys. Rev. B 58 (1998) R5901.
[18] J.M. De Teresa, M.R. Ibarra, J. Blasco, J. García, C. Marquina, P.A. Algarabel, Z. Arnold, K. Kamenev, C. Ritter, R. von Helmolt, Phys. Rev. B 54 (1996) 1187.
[19] S.R. Barman, A. Chainani, D.D. Sarma, Phys. Rev. B 49 (1994) 8475.
[20] T. Mizokawa, A. Fujimori, T. Arima, Y. Tokura, N. Mori, J. Akimitsu, Phys. Rev. B 52 (1995) 13865.
[21] W. Low, Phys. Rev. 109 (1958) 247.
[22] J.E. Gulley, V. Jaccarino, Phys. Rev. B 6 (1972) 58.
[23] J.A. Fernandez-Beca, P. Dai, H. Kawano-Furukawa, H. Yoshizawa, E.W. Plummer, S. Katano, T. Tomioka, Y. Tokura, Phys. Rev. B 66 (2002) 054434.
[24] C. Zener, Phys. Rev. 82 (1951) 403.
[25] L. Pi, L. Zhang, Y. Zhang, Phys. Rev. B 61 (2000) 8917.
[26] P. Schiffer, A.P. Ramirez, W. Bao, S.W. Cheong, Phys. Rev. Lett. 75 (1995) 3336.
[27] G.J. Snyder, R. Hiskes, S. Dicarolis, M.R. Beasley, T.H. Geballe, Phys. Rev. B 53 (1996) 14434.
[28] N.F. Mott, E.A. Davis, in: Electronics Process in Non Crystalline Materials, Clarendon press, Oxford, 1971.
[29] L. Ferro, J. Lukatela, B. Keszei, Solid State Commun. 73 (1990) 501.
[30] A. Urushibara, et al., Phys. Rev. B 51 (1995) 14103.